International Journal of Solids and Structures 50 (2013) 186–200

Contents lists available at SciVerse ScienceDirect

International Journal of Solids and Structures

journal homepage: www.elsevier.com/locate/ijsolstr

The stress intensity factors for a periodic array of interacting coplanar penny-shaped cracks

Huseyin Lekesiz [a,1], Noriko Katsube [a,*], Stanislav I. Rokhlin [b], Robert R. Seghi [c]

[a] Department of Mechanical and Aerospace Engineering, The Ohio State University, Columbus, OH, USA
[b] Department of Materials Science and Engineering, The Ohio State University, Columbus, OH, USA
[c] College of Dentistry, The Ohio State University, Columbus, OH, USA

ARTICLE INFO

Article history:
Received 6 February 2012
Received in revised form 8 August 2012
Available online 10 October 2012

Keywords:
Stress intensity factor
Coplanar penny-shaped crack
Periodic array
Interacting cracks

ABSTRACT

The effect of crack interactions on stress intensity factors is examined for a periodic array of coplanar penny-shaped cracks. Kachanov's approximate method for crack interactions [Kachanov, M., 1987. Elastic solids with many cracks: a simple method of analysis. International Journal of Solids and Structures 23 (1), 23–43] is employed to analyze both hexagonal and square crack configurations. In approximating crack interactions, the solution converges when the total truncation number of the cracks is 10^9. As expected, due to high density packing crack interaction in the hexagonal configuration is stronger than that in the square configuration. Based on the numerical results, convenient fitting equations for quick evaluation of the mode I stress intensity factors are obtained as a function of crack density and angle around the crack edge for both crack configurations. Numerical results for the mode II and III stress intensity factors are presented in the form of contour lines for the case of Poisson's ratio $\nu = 0.3$. Possible errors for these problems due to Kachanov's approximate method are estimated. Good agreement is observed with the limited number of results available in the literature and obtained by different methods.

1. Introduction

Problems related to interactions of multiple penny-shaped cracks have wide application in analyzing damage mechanisms of brittle materials such as concrete, rocks and ceramics. Such an interaction is also important in assessing the integrity of interfaces in bonded structures. In brittle materials, discontinuous macro-flaws can be idealized as multiple penny-shaped cracks in the plane of the eventual fracture and the progressive damage can be modeled by the growth of these cracks. Bonded interfaces are subjected to various mechanical loads and environmental factors (Lavrentyev and Rokhlin, 1994), and initial flaws and their progressive growth can be modeled by multiple penny-shaped cracks at the interface.

The stress fields generated by a single penny-shaped crack loaded by a uniform normal or shear load are usually given in terms of integrals of Bessel functions (Sneddon and Lowengrub, 1969). For a variety of loadings, Fabrikant (1990) has derived new single crack solutions in elementary functions. He has also proposed (Fabrikant, 1987, 1989) a new method for the stress analysis of an elastic space weakened by several arbitrarily located coplanar circular cracks. The method is based on a new type of integral equations which are non-singular and the iteration procedure is shown to be rapidly convergent even for closely spaced cracks.

Kachanov (1985, 1987, 1994, 2003) developed a simple method of stress analysis for elastic solids with many cracks, which are applicable to both two- and three-dimensional crack interaction problems. The method is based on stress superposition and the problem is formulated in terms of interaction functions. Considering the action of the *j*th crack on the *k*th crack, an approximation is made by assuming uniform traction on the *j*th crack, thus neglecting the second order effect of the *k*th crack on the *j*th crack traction distribution. Utilizing Fabrikant's (1990) stress solution for a penny-shaped crack loaded by uniform tractions, Kachanov and Laures (1989) applied Kachanov's method to three dimensional problems of strongly interacting penny-shaped cracks and verified their results against Fabrikant's (1987, 1989) numerically evaluated exact solutions for two coplanar cracks. Recently, Zhan and Wang (2006) obtained new numerical results based on Legendre polynomial representations of displacements and the boundary collocation method. They have compared their results for two coplanar cracks with those of Kachanov and Laures (1989) and Fabrikant (1987) and found good agreement.

A limited number of publications concerning crack interactions of a doubly periodic array of penny-shaped cracks is available. Sekine and Mura (1979) approached this problem based on the

* Corresponding author. Tel.: +1 614 292 0971; fax: +1 614 292 3163.
E-mail address: katsube.1@osu.edu (N. Katsube).
[1] Current address: Department of Mechanical Engineering, Bursa Technical University, Bursa, Turkey.

0020-7683/$ - see front matter © 2012 Elsevier Ltd. All rights reserved.
http://dx.doi.org/10.1016/j.ijsolstr.2012.09.018

Somigliana dislocation method, and approximate solutions for the mode I, II and III SIFs were presented by truncating the series in displacement gradients. Huang and Karihaloo (1992) examined this problem based on a Fredholm integral equation of the second kind. The crack interactions were formulated based on displacement averages instead of Kachanov's (1987) traction averages. The results with normal loading were obtained and the average stress intensity factor was presented.

In this work, the approximate method developed by Kachanov and his coworkers (1985, 1987, 1989, 1994) is applied to the problem of an array of doubly periodic coplanar cracks with square and hexagonal configurations (Fig. 1(b) and (c)) in an infinite medium subjected to remote tension and shear (Fig. 1(a)). The hexagonal crack configuration is important since the number of cracks per unit area (given the same crack radius and periodicity) is the highest and crack interactions in the hexagonal configuration are anticipated to be higher than those in other crack configurations. The mode I, II and III stress intensity factors (SIFs) are calculated; the convergence error of the solution is quantified as a function of crack density and direction angle along the crack edge. For the mode I SIF, simple fitting functions of numerical results are obtained (with the crack density and the direction angle as parameters). For the mode II and III SIFs, the numerical results are presented in the form of contour lines for the case of Poisson's ratio $\nu = 0.3$. Possible errors due to Kachanov's approximate method itself as it applies to these problems are estimated. It is also shown that the normalized mode I, II, and III SIFs are identical under the assumption of widely spaced cracks. Good agreement was observed with the limited number of results available in the literature and obtained by different methods.

2. Normal loading

2.1. Formulation for the mode I stress intensity factor

In this section, we apply the approximate method of Kachanov and Laures (1989) to the analysis of interacting cracks to obtain the mode I SIF of an array of periodic coplanar penny-shaped cracks in an infinite medium subjected to a remote normal traction at infinity, Fig. 1(a). The surfaces of the cracks are stress free. Square, Fig. 1(b), and hexagonal, Fig. 1(c), configurations of cracks are considered; a is the crack radius and b is the crack periodicity ($2b$ is the distance between centers of two adjacent cracks). For both square and hexagonal configurations cracks are numbered counterclockwise according to the distance from the center of crack #1. Let us for a moment consider a large number of cracks N and later let N approach infinity. Following Kachanov (1985, 1987), first the problem with remote loading is replaced by crack faces loaded with tractions and vanishing stresses at infinity. Second, based on the stress superposition the problem is separated into N problems, each containing a single crack loaded by unknown tractions resulting from the action of the other cracks. Without loss of generality, we choose to determine a distribution of the unknown traction on

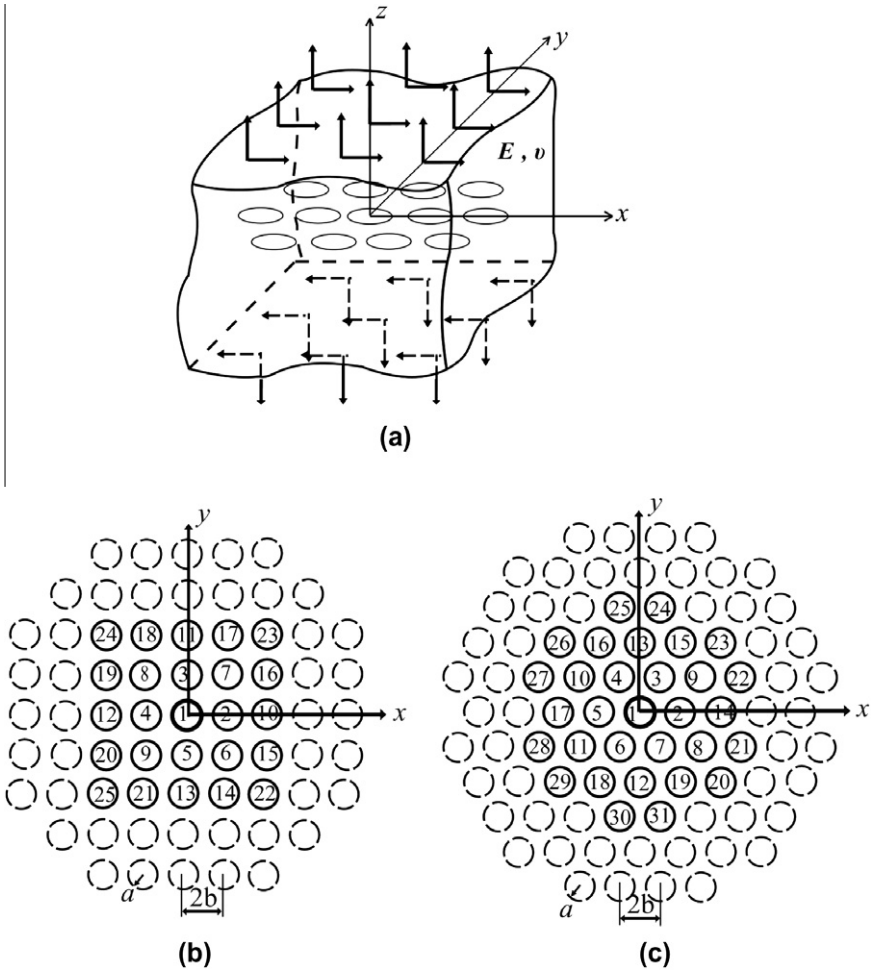

Fig. 1. (a) An array of periodic coplanar penny shaped cracks in an infinite medium subjected to remote tension and shear, (b) square configuration of cracks, (c) hexagonal configuration of cracks.

the surface of crack #1 and the corresponding SIF as summarized below.

Let us select one of these N problems (problem j) and consider a single penny-shaped crack #j of radius a in an infinite homogenous material subjected to a uniform unit traction as shown in Fig. 2. The axisymmetric stress $(\sigma_{zz})_j$ in the crack plane ($z = 0$) is given by Kachanov and Laures (1989) and Fabrikant (1990) as

$$\overline{\sigma_j}(\overline{\rho_j}) = \frac{2}{\pi}\left[\frac{1}{\sqrt{\overline{\rho_j}^2 - 1}} - \sin^{-1}\left(\frac{1}{\overline{\rho_j}}\right)\right], \tag{1}$$

where $\overline{\rho_j} = \rho_j/a$ and ρ_j is the radial distance measured from the center of crack #j.

Next the average stress Λ_{j1}^{zz} due to crack #j acting on the imaginary crack #1 is determined. It is termed the transmission factor (Kachanov and Laures, 1989):

$$\Lambda_{j1}^{zz} = \frac{1}{\pi a^2}\int\int_{S_1}\overline{\sigma_j}(\rho_j)dS_1, \quad j = 1,2,3,\ldots, \tag{2}$$

where S_1 represents the surface of the imaginary crack #1 in its local coordinates $\overline{\rho_1}(=\rho_1/a)$ and ϕ_1 (Fig. 2). The first index in the superscript 'zz' in Eq. (2) indicates the direction of the traction applied on the real crack #j surface, the second indicates that of the traction averaged over the imaginary crack #1 region.

Combining all N problems and letting $N \to \infty$, the average traction for crack #1, $\langle p_1\rangle$, can be written for an infinite number of coplanar cracks as the sum of the applied load p^0 and the effect of all the surrounding cracks.

$$\langle p_1\rangle = p^0 + \Lambda_{21}^{zz}\langle p_2\rangle + \Lambda_{31}^{zz}\langle p_3\rangle + \cdots\cdots\cdots + \Lambda_{j1}^{zz}\langle p_j\rangle + \cdots\cdots\cdots, \tag{3}$$

where $\langle p_j\rangle$ ($j = 1,2,3,\ldots$) is the average traction for crack #j and is yet unknown. For periodic configurations of an infinite number of cracks as in Fig. 1(b) and (c), average tractions $\langle p_j\rangle$ are the same for all the cracks

$$\langle p_1\rangle = \langle p_2\rangle = \langle p_3\rangle = \langle p_4\rangle = \cdots\cdots\cdots\cdots\cdots = \langle p\rangle. \tag{4}$$

Eqs. (3) and (4) lead to

$$\frac{\langle p\rangle}{p^0} = \frac{1}{1 - \sum_{j=2}^{\infty}\Lambda_{j1}^{zz}}. \tag{5}$$

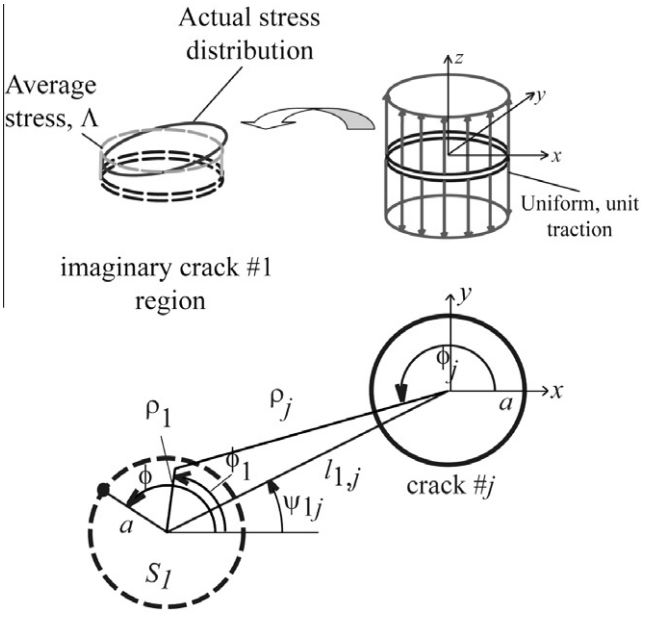

Fig. 2. Model of crack interactions and coordinate system for Eqs. (2), (6) and (7).

Physically Eq. (5) represents a convergent geometric progression of crack interactions with resulting averaged traction $\langle p\rangle$ increase over p^0. The traction distribution on the crack #1 surface then can be written as

$$\begin{aligned} p_1(\overline{\rho_1},\phi_1) &= p^0 + \langle p\rangle\overline{\sigma_2}(\overline{\rho_1},\phi_1) + \langle p\rangle\overline{\sigma_3}(\overline{\rho_1},\phi_1) + \cdots\cdots \\ &= p^0\left(1 + \frac{\langle p\rangle}{p^0}\sum_{j=2}^{\infty}\overline{\sigma_j}(\overline{\rho_1},\phi_1)\right), \end{aligned} \tag{6}$$

where $\overline{\sigma_j}(\overline{\rho_1},\phi_1)$ is the stress distribution in the region occupied by crack #1 due to crack #j, and is defined by Eq. (1) in the local coordinates of crack #1. The obtained traction acting on crack #1 is non-uniform. Note that the only approximation made is that the stress distribution $\overline{\sigma_j}(\overline{\rho_1},\phi_1)$, appearing in (5) and (6) from the action of crack #j and obtained from Eq. (1), is for uniform traction distribution on crack #j; in reality due to the effect of other cracks this traction is not uniformly distributed, and as done by Kachanov (1985, 1987) the effect of this non-uniformity is neglected.

The mode I SIF at the given point ϕ of the edge of a crack due to arbitrary distribution of the normal traction $p_1(\overline{\rho_1},\phi_1)$ is given by Eq. (2.5) in Kachanov and Laures (1989).

$$\frac{K_I(\phi)}{K_I^0} = \frac{1}{2\pi}\int_0^{2\pi}\int_0^1 \frac{\sqrt{1-\overline{\rho_1}^2}\,\overline{p_1}(\overline{\rho_1},\phi_1)\overline{\rho_1}d\overline{\rho_1}d\phi_1}{1+\overline{\rho_1}^2 - 2\overline{\rho_1}\cos(\phi-\phi_1)}, \tag{7}$$

where the normalization factor $K_I^0 = p^0\sqrt{2a}/\pi$ is the SIF for a crack loaded by a uniform normal pressure p^0, and $\overline{p_1}(\overline{\rho_1},\varphi_1) = p_1(\overline{\rho_1},\varphi_1)/p^0$. The fact that that the SIF is given as an integral over the crack surface results in its low sensitivity to the approximations involved in the use of a uniform traction distribution on crack #j to obtain tractions $\overline{\sigma_j}(\overline{\rho_1},\varphi_1)$, Eq. (1), and thus to the effect of minor deviations of the traction distribution $p_1(\overline{\rho_1},\varphi_1)$, Eq. (6), from the exact as long as its average is accurate.

2.2. Approximation of the crack interaction: convergence of the solution and crack number truncation

For computation of the SIF (7), one needs to bound the total number of cracks in Eq. (6), so that the infinite series in Eqs. (5) and (6) are truncated at m. As we will see below the convergence of Eqs. (5) and (6) is slow and the total truncation number of cracks m is very large. With increase of distance between crack #j and #1, the stress distribution term from the action of crack #j over crack #1, $\overline{\sigma_j}(\overline{\rho_1},\phi_1)$, becomes flat and can be replaced by a constant. In particular, we approximate in Eq. (6) the stress distribution $\overline{\sigma_j}(\overline{\rho_1},\varphi_1)$ attributed to cracks located sufficiently far from crack #1 ($j > n$) by its value at the crack #1 center, $\bar{\sigma}_j^0 = \overline{\sigma_j}(0,0)$

$$\bar{\sigma}_j(\bar{\rho}_1,\phi_1) = \bar{\sigma}_j^0 = \overline{\sigma_j}(\bar{\rho}_1 = 0,\phi_1 = 0) = const \quad \text{for} \quad m \geqslant j > n. \tag{8}$$

Eq. (8) reduces the number of cracks in Eqs. (5) and (6) for which the exact stress distribution $\bar{\sigma}_j = \overline{\sigma_j}(\overline{\rho_1},\varphi_1)$ is accounted for over crack #1; we call this number, n, the transition number ($n < m$).

The suitability of approximation (8) is illustrated in Fig. 3 and will be evaluated in Section 2.2.1. When the stress distribution can be approximated by its constant value at the crack #1 center as in Eq. (8), integration of the stress distribution over the crack #1 area in Eq. (2) becomes unnecessary since $\Lambda_{j1}^{zz}(\bar{\sigma}_j)$ becomes the constant $\bar{\sigma}_j^0$. This approximation for $j > n$ significantly reduces the computation costs, and Eqs. (5) and (6) are rewritten after the truncation as follows:

$$\frac{\langle p\rangle}{p^0} \approx \frac{1}{1 - \sum_{j=2}^{n}\Lambda_{j1}^{zz}(\bar{\sigma}_j) - \sum_{j=n+1}^{m}\bar{\sigma}_j^0} \tag{9}$$

$$p_1(\overline{\rho_1},\varphi_1) \approx p^0\left[1 + \frac{\langle p\rangle}{p^0}\left(\sum_{j=2}^{n}\bar{\sigma}_j + \sum_{j=n+1}^{m}\bar{\sigma}_j^0\right)\right] \tag{10}$$

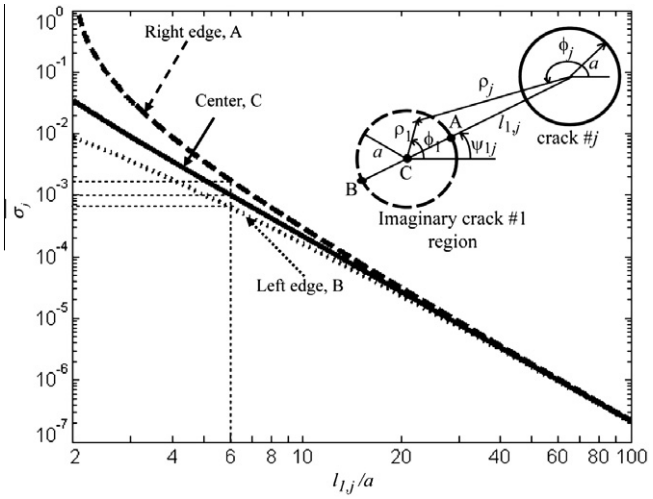

Fig. 3. The normal stress values at points A (the nearest), B (the furthest) and C (the center) in the imaginary crack #1 region due to the unit normal traction applied at the crack #*j* face as a function of $l_{1,j}/a$ ($l_{1,j}$: center to center distance, *a*: crack radius).

2.2.1. The transition number n

In order to determine the transition number n defined by Eq. (8), we have compared in Fig. 3 the stress $\overline{\sigma_j}(\overline{\rho_1}, \phi_1)$ at three points of the imaginary crack #1 versus the normalized crack distance, $l_{1,j}/a$; the points A ($\rho_1 = a$, $\phi_1 = \psi_{1j}$), B ($\rho_1 = a$, $\phi_1 = \psi_{1j} + \pi$) and C ($\rho_1 = 0$, $\phi_1 = 0$) are indicated in Fig. 3. The distance between the two crack centers and the angle measured counterclockwise from the x axis to the center of crack #j, respectively, are denoted by $l_{1,j}$ and ψ_{1j}. As $l_{1,j}/a$ becomes large, the maximum and minimum stresses represented by A (dashed line) and B (dotted line) become identical and both quickly decay. For $l_{1,j}/a$ = 4,6,12, the normalized stress values at the center C are, respectively, 0.003513, 0.001008, 0.0001236, which are significantly smaller than the unit traction applied to the crack # j. The condition for normalized crack distance $l_{1,j}/a \geqslant$ 4,6,12, respectively, is satisfied for all cracks numbered larger than 9, 25, 109 in the square configuration and 13, 31, 121 in the hexagonal configuration (Fig. 1(b) and (c)). Based on this consideration, n in Eq. (10) is chosen to be 25 and 31 for the square and hexagonal configurations respectively (for these n values the normalized stress value at crack #1 center reduces to the order of 10^{-3}).

2.2.2. The truncation number m

To determine the truncation number m of the total number of cracks, we have examined the convergence of both Eqs. (9) and (10). Focusing first our attention on Eq. (10) we have displayed in Fig. 4 the sum of the normalized stresses $\sum_{j=n+1}^{m} \bar{\sigma}_j^0$ versus m for the square (Fig. 4(a), n = 25) and hexagonal (Fig. 4(b), n = 31) configurations. Since the truncation number m is determined by the number of cracks located within the circular region bounded by the maximum normalized distance l/a, the parameter l/a is indicated above the axis m in the figure. The example is given for the crack density a/b = 0.99 which corresponds to the slowest convergence for the crack density range $0 < a/b < 0.99$ studied (this covers most practical cases).

For the same a/b ratio, the stress summation, $\sum_{j=n+1}^{m} \overline{\sigma_j}(0,0)$, for the hexagonal configuration is larger than that for the square configuration since cracks in the hexagonal configuration are more closely packed. Even though stress reduces significantly far from the crack, the convergence is very slow, Fig. 4. Not even two digits are stabilized between $l_{1,j}/a$ = 101.01 and $l_{1,j}/a$ = 505.05 with corresponding m = 7824 and 196292 for the square configuration and m = 8584 and 213868 for the hexagonal configuration. While the normalized stress from a single crack #j decays asymptotically as distance cubed, the number of cracks located within the circular area bounded by a specific distance increases as distance squared. Therefore the total stress decays inversely with the distance and the convergence is very slow as also discussed in Appendix A.

The stabilization to the first four effective digits in the sums is achieved at $m = 10^9$ and $m = 10^{10}$ where the sums $\sum_{j=n+1}^{m} \overline{\sigma_j}(0,0)$ reach values 0.05785 and 0.06442 for the square and hexagonal configurations, respectively. Since the convergence of Eq. (10) requires that of Eq. (9) we chose at this stage the truncation number $m = 10^9$, which will be discussed more below.

In our original assumption of a periodic arrangement of an infinite number of cracks, due to symmetry each crack has the same stress state that results in Eqs. (4)–(6). When the number of cracks is bounded by the truncation number m, the stress state of the edge and near-edge cracks of the crack array is different and equality (4) is not valid for all cracks. As the number of cracks m increases, the number of inner cracks grows as m while the number of edge cracks grows as $\sqrt{m}$. When the process converges, $m = 10^9$, the edge effect is negligible.

2.2.3. Impact of transition number on the SIF

The error on the SIF in Eq. (7) of truncation with the transition number n is obtained by substituting Eqs. (9) and (10) into Eq. (7) and comparing the truncation results in two cases: (1) taking the transition bounds n = 25 and 31 in computations for the square and hexagonal configurations and (2) performing computations with transition bounds n = 109 and 121 for square and hexagonal configurations respectively while keeping $m = 10^9$ constant. The maximum error is found to be less than 0.0864%. Therefore, n = 25 and 31 for the square and hexagonal configurations and $m = 10^9$ are chosen for all other calculations of the SIF.

2.3. The normalized mode I SIF evaluated as a function of a/b and ϕ and the corresponding curve fitting function

The normalized mode I SIF as a function of a/b and ϕ are shown by solid circles in Fig. 5(a) and (b). Calculations are performed for the range of crack density $0 \leqslant a/b \leqslant 0.99$ for both configurations. The numerical error by truncating the total number of cracks at $m = 10^9$ is not significant as discussed in Section 2.2, but it becomes larger for $a/b > 0.99$.

For $a/b < 0.5$, in both configurations, $K_I(\phi)/K_I^0$ remains close to one for all values of ϕ, indicating almost no crack interaction. The normalized SIF increases as a/b increases and the angle ϕ approaches zero. As expected, crack interactions in the hexagonal configuration are stronger than those in the square configuration.

The following empirical equations are obtained by surface fitting the numerical results based on the least square method.

$$\frac{K_I^{\infty,surface-fit}\left(\frac{a}{b},\phi\right)}{K_I^0} = 1 + 0.2907 \ln\left[\sec\left\{1.5142\left(\frac{a}{b}\right)^2\right\}\right]\sqrt{|\cos\phi|} + 0.0376 \tan\left[1.5558\left(\frac{a}{b}\right)^2 \cos^2\phi\right] \quad (11)$$

for the square configuration,

$$\frac{K_I^{\infty,surface-fit}\left(\frac{a}{b},\phi\right)}{K_I^0} = 1 + 0.3794 \ln\left[\sec\left\{1.5572\left(\frac{a}{b}\right)^2\right\}\right]\sqrt{|\cos(\phi)|} + 0.06297 \tan\left[1.5508\left(\frac{a}{b}\right)^3 \cos^3(\phi)\right] \quad (12)$$

for the hexagonal configuration.

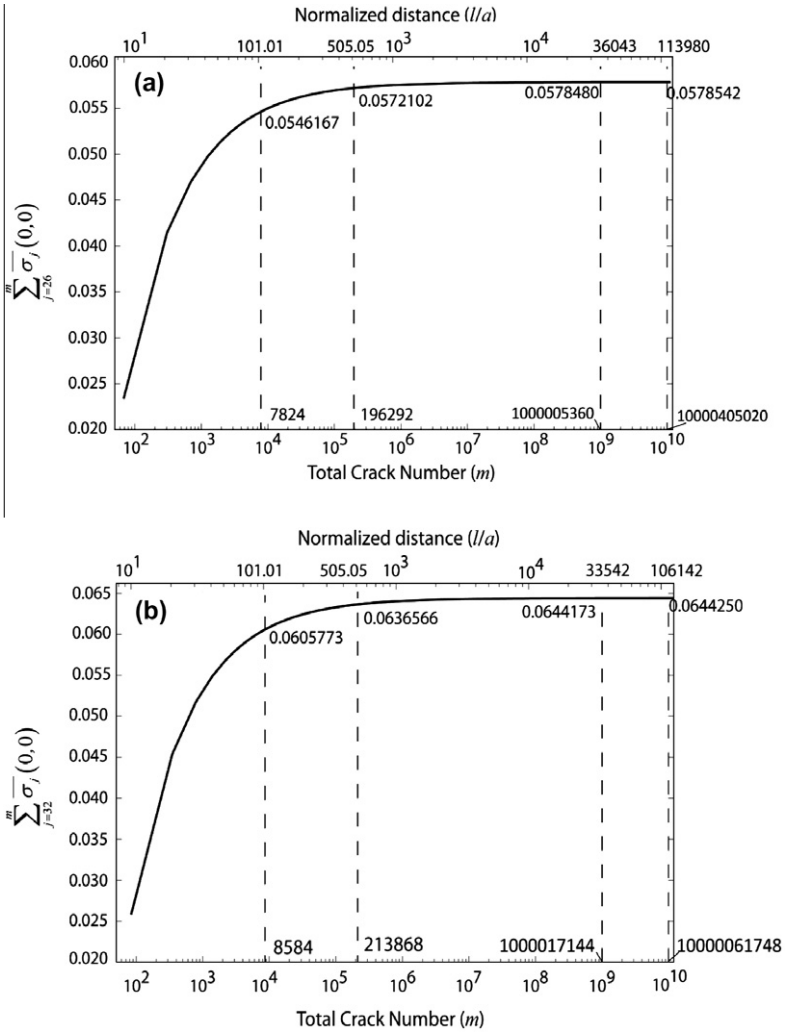

Fig. 4. The sum of the normalized stress evaluated at the center of crack #1 due to unit traction acting on a face of crack #*j* versus the total crack number, *m*: (a) square configuration of cracks (b) hexagonal configuration. Corresponding normalized distance *l*/*a* is indicated above the axis *m*; crack density is *a*/*b* = 0.99.

The error of the fitting functions (11) and (12) are shown in Fig. 6 as a function of parameters a/b and ϕ. The maximum errors for the square, Fig. 6(a), and hexagonal, Fig. 6(b), configurations are, respectively, 2.46% and 3.04% and occur at the range of $a/b > 0.8$. Eqs. (11) and (12) provide convenient tools for quick evaluation of the SIF of an infinite number of interacting coplanar cracks for the square and hexagonal configurations as a function of ϕ and a/b for $0 \leqslant a/b \leqslant 0.99$.

3. Transverse loading

3.1. Formulation of the mode II and III SIFs

In this section, we extend our analysis to the case where an infinite number of coplanar cracks are subjected to a remote constant shear traction as shown in Fig. 1(a). This problem is replaced by an equivalent problem where crack faces are subjected to traction t_0 in the x direction and stresses vanishing at infinity. As in the normal traction case, we start with the equivalent problem of N cracks which is separated into N problems where each contains a single crack (later we let N approach to infinity). A constant shear traction applied to an isolated single crack in the x direction produces a shear stress distribution both in the x and y directions around that crack which affects the stress distribution in the vicinity of all other cracks. Due to this coupling, in the calculation of the transmission factor we need to employ the stress field around a single crack (crack #j) subjected to a constant shear in both directions, t^0 in the x direction and s^0 in the y direction. The shear stress distribution outside the crack is given by Eq. (44) in Sankar and Fabrikant (1983) as follows.

$$\tau_j^x(\overline{\rho_j},\phi_j)+i\tau_j^y(\overline{\rho_j},\phi_j)=\frac{2(t^0+is^0)}{\pi}\left[\frac{1}{\sqrt{\overline{\rho_j}^2-1}}-\sin^{-1}\frac{1}{\overline{\rho_j}}\right]+\frac{2(t^0-is^0)}{\pi}\frac{v}{2-v}\left(\frac{\cos 2\phi_j+i\sin 2\phi_j}{\overline{\rho_j}^2\sqrt{\overline{\rho_j}^2-1}}\right), \tag{13}$$

where τ_j^x and τ_j^y, respectively, are the shear stresses in the x and y directions around the crack #j and v is the Poisson's ratio of the material.

Similar to the normal loading case (Eq. (3)), we consider the action of various "j" cracks on crack #1. The average shear traction at the crack #1 in the x and y directions, $\langle t_1\rangle$, $\langle s_1\rangle$, respectively, can be written as follows.

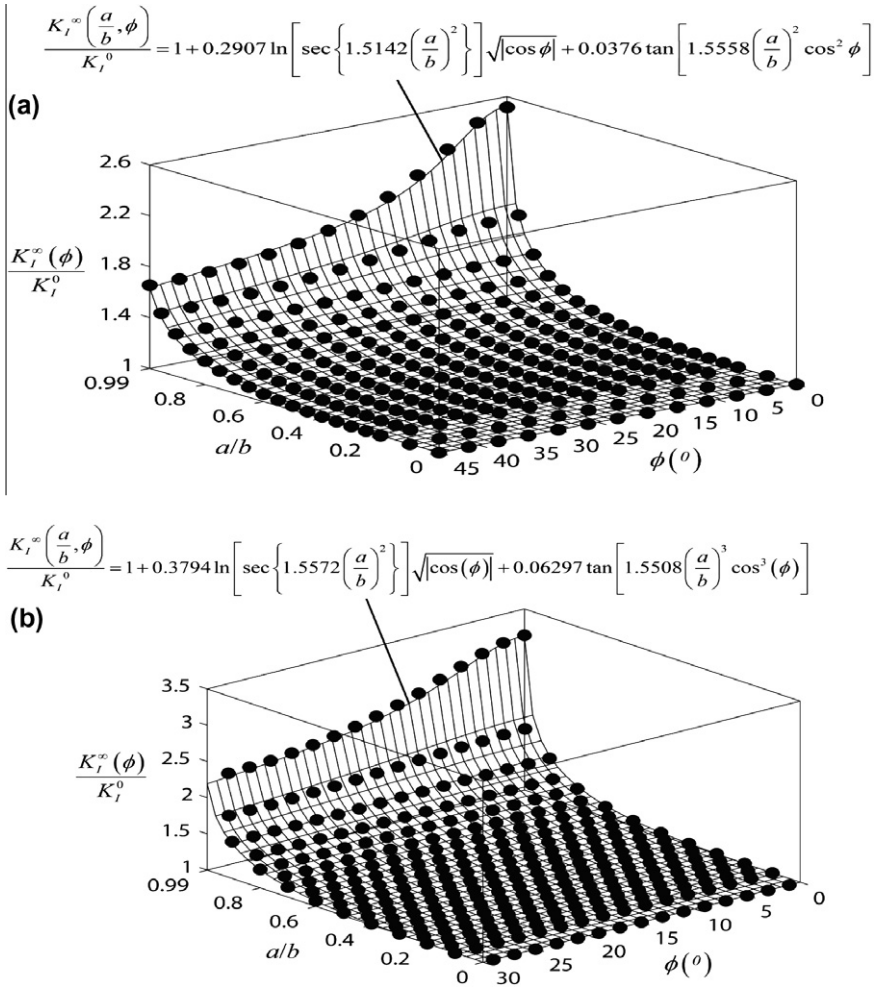

Fig. 5. The normalized mode I SIF for a periodic array of coplanar penny-shaped cracks as a function of angle around the crack circumference ϕ and crack density parameter a/b; calculations are indicated by circular dots; the corresponding fitted surface is also shown: (a) the square and (b) the hexagonal configurations. The normalization factor K_I^0 is the SIF for an isolated crack.

$$\begin{aligned}\langle t_1\rangle &= t^0 + \Lambda_{21}^{xx}\langle t_2\rangle + \Lambda_{31}^{xx}\langle t_3\rangle + \cdots\cdots\cdots + \Lambda_{21}^{yx}\langle s_2\rangle + \Lambda_{31}^{yx}\langle s_3\rangle + \cdots\cdots\\ \langle s_1\rangle &= \Lambda_{21}^{xy}\langle t_2\rangle + \Lambda_{31}^{xy}\langle t_3\rangle + \cdots\cdots\cdots + \Lambda_{21}^{yy}\langle s_2\rangle + \Lambda_{31}^{yy}\langle s_3\rangle + \cdots\cdots,\end{aligned} \tag{14}$$

where $\langle t_j\rangle$ and $\langle s_j\rangle$ ($j = 1,2,3,\ldots$) are the (unknown) average tractions for crack #j and Λ represents the corresponding transmission factor. The first and second subscripts for Λ, respectively, indicate crack #j and crack #1. The first and second superscripts for Λ, respectively, indicate the direction of the unit shear stress applied on crack #j surface and that of the stress averaged over the crack #1 region.

Based on Eq. (13) the transmission factor Λ_{j1}^{xy} and Λ_{j1}^{yx} are as follows:

$$\begin{aligned}\Lambda_{j1}^{xy} &= \frac{1}{\pi a^2}\int\int_{S_1}\overline{\tau}_j^{\,y}(\overline{\rho}_j,\phi_j)\Big|_{s^0=0} dS_1,\\ \Lambda_{j1}^{yx} &= \frac{1}{\pi a^2}\int\int_{S_1}\overline{\tau}_j^{\,x}(\overline{\rho}_j,\phi_j)\Big|_{t^0=0} dS_1,\end{aligned} \tag{15a}$$

where

$$\overline{\tau}_j^{\,x}(\overline{\rho}_1,\phi_1)\big|_{t^0=0} = \frac{\tau_j^x(\overline{\rho}_1,\phi_1)\big|_{t^0=0}}{s^0}, \quad \overline{\tau}_j^{\,y}(\overline{\rho}_1,\phi_1)\big|_{s^0=0} = \frac{\tau_j^y(\overline{\rho}_1,\phi_1)\big|_{s^0=0}}{t^0}. \tag{15b}$$

The factors Λ_{j1}^{xy} and Λ_{j1}^{yx} can be shown to be identical

$$\Lambda_{j1}^{xy} = \Lambda_{j1}^{yx} = \frac{1}{\pi a^2}\int\int_{S_1}\frac{2}{\pi}\left(\frac{\nu}{2-\nu}\right)\left(\frac{\sin 2\phi_j}{\overline{\rho}_j^2\sqrt{\overline{\rho}_j^2-1}}\right)dS_1. \tag{16}$$

Similarly, Λ_{j1}^{xx} and Λ_{j1}^{yy} can be expressed as

$$\begin{aligned}\Lambda_{j1}^{xx} &= \frac{1}{\pi a^2}\int\int_{S_1}\overline{\tau}_j^{\,x}(\overline{\rho}_j,\phi_j)\Big|_{s^0=0} dS_1\\ &= \frac{1}{\pi a^2}\int\int_{S_1}\frac{2}{\pi}\left\{\left[\frac{1}{\sqrt{\overline{\rho}_j^2-1}} - \sin^{-1}\frac{1}{\overline{\rho}_j}\right] + \frac{\nu}{2-\nu}\left(\frac{\cos 2\phi_j}{\overline{\rho}_j^2\sqrt{\overline{\rho}_j^2-1}}\right)\right\}dS_1,\\ \Lambda_{j1}^{yy} &= \frac{1}{\pi a^2}\int\int_{S_1}\overline{\tau}_j^{\,y}(\overline{\rho}_j,\phi_j)\Big|_{t^0=0} dS_1\\ &= \frac{1}{\pi a^2}\int\int_{S_1}\frac{2}{\pi}\left\{\left[\frac{1}{\sqrt{\overline{\rho}_j^2-1}} - \sin^{-1}\frac{1}{\overline{\rho}_j}\right] - \frac{\nu}{2-\nu}\left(\frac{\cos 2\phi_j}{\overline{\rho}_j^2\sqrt{\overline{\rho}_j^2-1}}\right)\right\}dS_1,\end{aligned} \tag{17}$$

where

$$\begin{aligned}\overline{\tau}_j^{\,x}(\overline{\rho}_1,\phi_1)|_{s^0=0} &= \frac{\tau_j^x(\overline{\rho}_1,\phi_1)|_{s^0=0}}{t^0},\\ \overline{\tau}_j^{\,y}(\overline{\rho}_1,\phi_1)|_{t^0=0} &= \frac{\tau_j^y(\overline{\rho}_1,\phi_1)|_{t^0=0}}{s^0}.\end{aligned} \tag{18}$$

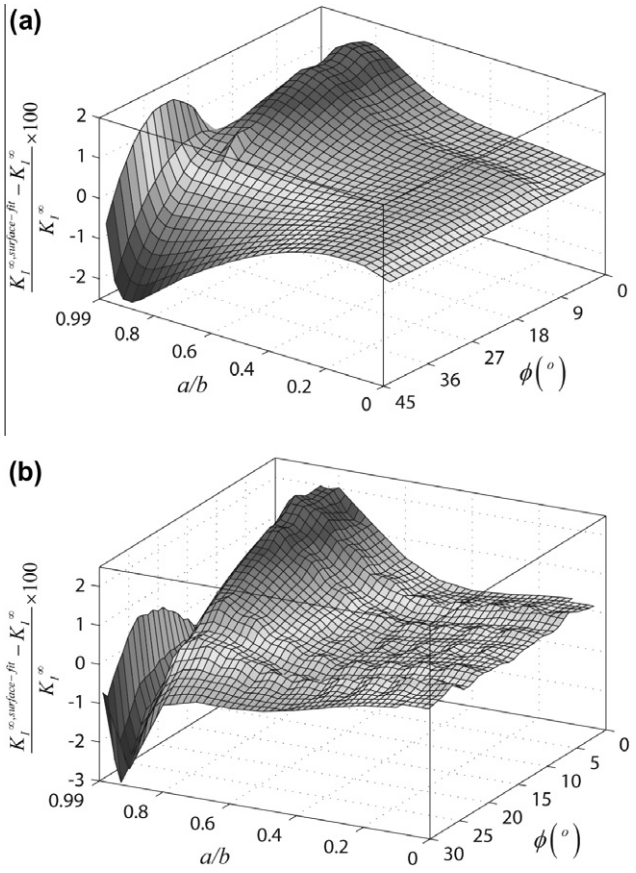

Fig. 6. Error (in percent) of the surface fitting, Eqs. (11) and (12), of the mode I SIF (Fig. 5): (a) the square (b) the hexagonal configurations for the periodic array of penny-shaped cracks.

For an infinite number of cracks with a periodic configuration, average tractions, $\langle t_j \rangle$ and $\langle s_j \rangle$ are identical for all cracks. Therefore, we can write

$$\begin{aligned} &\langle t_1 \rangle = \langle t_2 \rangle = \langle t_3 \rangle = \langle t_4 \rangle = \cdots\cdots = \langle t \rangle, \\ &\langle s_1 \rangle = \langle s_2 \rangle = \langle s_3 \rangle = \langle s_4 \rangle = \cdots\cdots = \langle s \rangle. \end{aligned} \tag{19}$$

Eqs. (14) and (19) lead to the following system of equations

$$\begin{bmatrix} 1-\sum_{j=2}^{\infty} \Lambda_{j1}^{xx} & -\sum_{j=2}^{\infty} \Lambda_{j1}^{yx} \\ -\sum_{j=2}^{\infty} \Lambda_{j1}^{xy} & 1-\sum_{j=2}^{\infty} \Lambda_{j1}^{yy} \end{bmatrix} \begin{Bmatrix} \langle t \rangle \\ \langle s \rangle \end{Bmatrix} = \begin{Bmatrix} t^0 \\ 0 \end{Bmatrix} \tag{20}$$

Next, we will demonstrate that due to periodicity the total effect on summation of the transmission factors (16) Λ_{j1}^{xy} and Λ_{j1}^{yx} and the second terms in Eq. (17) (terms depending on Poisson's ratio) are zero. In the square crack configuration, there are multiple rows of four cracks squarely located at the same distance where the difference of angle ψ_{1j} (see Fig. 2) between two adjacent cracks among the four cracks is 90°. As summarized in Appendix B, by considering the four infinitesimal areal element dS_1 (within the crack #1 region) which are located at the same normalized distance $\bar{\rho}_j = \rho/a$ and form the square configuration, the summation of $\frac{\cos 2\phi_j}{\bar{\rho}_j^2 \sqrt{\bar{\rho}_j^2 - 1}}$ for these four infinitesimal areal elements and that of $\frac{\sin 2\phi_j}{\bar{\rho}_j^2 \sqrt{\bar{\rho}_j^2 - 1}}$ vanish due to the fact that angle between two adjacent areal elements is 90° (see Fig. 16(a)). Therefore, if we integrate these terms over the crack #1 region as in Eqs. (16) and (17), the summation of the contribution due to these squarely located surrounding four cracks vanishes (see Eqs. (B3) and (B4)). It is important to note that the periodicity of crack configurations play a key role in obtaining this result. Similarly, as described in the Appendix B, taking advantage of the periodicity of the hexagonal crack configuration, the summation in the integral over the crack #1 region of the terms from the hexagonally-located surrounding six cracks also vanishes (see Fig. 16(b)). By applying this procedure to each layer of periodic crack configurations, it can be shown that the summation of Eq. (16) and the second term of the right hand side of Eq. (17) (the term with Poisson's ratio, ν) for an infinite number of cracks vanish. Noting that the first term of the right hand side of Eq. $(17)_{1,2}$ is identical to Λ_{j1}^{zz}, we obtain the following results which significantly simplify the summation of the transmission factors for the square and hexagonal crack configurations.

$$\sum_{j=2}^{\infty} \Lambda_{j1}^{yx} = \sum_{j=2}^{\infty} \Lambda_{j1}^{xy} = 0, \quad \sum_{j=2}^{\infty} \Lambda_{j1}^{xx} = \sum_{j=2}^{\infty} \Lambda_{j1}^{yy} = \sum_{j=2}^{\infty} \Lambda_{j1}^{zz}. \tag{21}$$

Inserting Eq. (21) into Eq. (20) and recalling Eq. (5), we obtain

$$\frac{\langle t \rangle}{t^0} = \frac{\langle p \rangle}{p^0} = \frac{1}{1 - \sum_{j=2}^{\infty} \Lambda_{j1}^{zz}}, \quad \langle s \rangle = 0. \tag{22}$$

Thus similar to Eq. (6), the traction distribution on the crack #1 surface is given by

$$\begin{aligned} t_1(\bar{\rho}_1, \phi_1) &= t^0 \left[1 + \frac{\langle t \rangle}{t^0} \sum_{j=2}^{\infty} \bar{\tau}_j^x(\bar{\rho}_1, \phi_1) \Big|_{s^0=0} \right], \\ s_1(\bar{\rho}_1, \phi_1) &= \langle t \rangle \sum_{j=2}^{\infty} \bar{\tau}_j^y(\bar{\rho}_1, \phi_1) \Big|_{s^0=0}. \end{aligned} \tag{23}$$

While in our case the remote shear traction component s^0 is zero, the pointwise stress distribution over crack #1 area has both t_1 and s_1 components. Also, it is important to note that the stress distribution depends on the Poisson's ratio ν, as results from Eqs. (13), (15b) and (18); only the averaged stress $\langle t \rangle$ (Eq. (22)), obtained by the integration over the crack #1 area, can be significantly simplified as in Eq. (21) and is independent of ν.

The infinite series in Eqs. (22) and (23) are truncated as in Eqs. (9) and (10) using the truncated number of cracks, m, and the transitional crack number, n, representing the nearby number of cracks for which the non-uniform stress distribution over the crack #1 is accounted for as follows:

$$t_1(\bar{\rho}_1, \phi_1) = t^0 \left[1 + \frac{\langle t \rangle}{t^0} \left(\sum_{j=2}^{n} \bar{\tau}_j^x(\bar{\rho}_1, \phi_1) \Big|_{s^0=0} + \sum_{j=n+1}^{m} \bar{\tau}_j^x(0,0) \Big|_{s^0=0} \right) \right], \tag{24}$$

$$s_1(\bar{\rho}_1, \phi_1) = \langle t \rangle \left(\sum_{j=2}^{n} \bar{\tau}_j^y(\bar{\rho}_1, \phi_1) \Big|_{s^0=0} + \sum_{j=n+1}^{m} \bar{\tau}_j^y(0,0) \Big|_{s^0=0} \right). \tag{25}$$

The mode II and III SIFs for crack#1 subjected to the traction of $(t_1 + i s_1)$ is given in Eq. (2.6) by Kachanov and Laures (1989) as follows.

$$\begin{aligned} K_{II}(\phi) + i K_{III}(\phi) = \frac{\sqrt{a}}{\pi^2 \sqrt{2}} \int_0^{2\pi} \int_0^1 \sqrt{1 - \overline{\rho_1}^2} \Bigg\{ &\frac{e^{-i\phi}(t_1 + i s_1)}{1 + \overline{\rho_1}^2 - 2\overline{\rho_1}\cos(\phi - \phi_1)} \\ &+ \frac{\nu}{2-\nu} \frac{e^{i\phi}(3 - \overline{\rho_1} e^{i(\phi-\phi_1)})(t_1 - i s_1)}{(1 - \overline{\rho_1} e^{i(\phi-\phi_1)})^2} \Bigg\} \overline{\rho_1} d\overline{\rho_1} d\phi_1, \end{aligned} \tag{26}$$

where the mode II and III SIFs for penny-shaped cracks depend on the Poisson's ratio ν. The mode II and III SIFs for a non-interacting crack subjected to traction t^0 in the x direction ($s^0 = 0$) are given by

$$K_{II}^{0}(\varphi) = \frac{4t^{0}\sqrt{a}}{\sqrt{2}\pi(2-\nu)}\cos(\varphi),$$
$$K_{III}^{0}(\varphi) = -\frac{4t^{0}\sqrt{a}(1-\nu)}{\sqrt{2}\pi(2-\nu)}\sin(\varphi). \quad (27)$$

The effect of m and n on the mode II and III SIFs are examined for the extreme case of $a/b = 0.99$ for the square and hexagonal configuration and $\nu = 0.5$ since it produces the largest error. The maximum error of the mode II and III SIF is determined at $m = 10^9$ by comparing the values for transition number $n = 25$ and 31 with that for $n = 109$ and 121 (for the square and hexagonal configurations respectively); the error is found to be less than 0.0892%. Therefore, $n = 25$ and 31 for the square and hexagonal configurations and $m = 10^9$ are chosen for further evaluation of the SIF.

3.2. The mode II and III SIFs as a function of a/b and ϕ

Fig. 7 shows contour lines for the normalized mode II SIF $K_{II}^{\infty}(\phi)/K_{II}^{0}(\phi = 0)$ for the square (a) and hexagonal (b) configurations as a function of the crack density parameter a/b and angle around the crack edge ϕ (the plots are for $\nu = 0.3$). Due to the symmetry of mode II SIF with respect to the x and y axes, the range of ϕ is bounded by $[0,90^{\circ}]$ for both configurations.

The effect of crack density a/b on the normalized mode II SIF is shown to be significant at $\phi = 0^{\circ}$ especially for the range $a/b > 0.6$. As a/b approaches zero, the normalized mode II SIF behaves like an isolated crack (see Eq. (27) $_1$). As a/b approaches one, the normalized mode II SIFs reach their maximum value at $\phi = 0^{\circ}$. Since crack interaction for the hexagonal configuration is stronger than for the square configuration, given the same a/b value, the SIF value for the hexagonal configuration ($\sim$3.294 for $a/b = 0.99$, $\phi = 0^{\circ}$) is larger than that for the square configuration ($\sim$2.655 for $a/b = 0.99$, $\phi = 0^{\circ}$). For all values of a/b, the normalized mode II SIFs diminishes as ϕ approaches 90° due to the symmetry of crack configurations with respect to the y axis.

As shown in Fig. 1(b) and (c), the center to center distance between crack #1 and crack #3 for the square and hexagonal configurations are $2\sqrt{2}b$ and $2b$, respectively, while the distance between crack #1 and crack #2 are $2b$ for both configurations. Therefore, crack #3 located at $\phi = 60^{o}$ for the hexagonal configuration contributes to a local peak for high crack densities ($\sim$1.645 for $a/b = 0.99$, $\phi = 0^{\circ}$ in Fig. 7(b)) while there is no local peak at $\phi = 45^{\circ}$ for the square configuration as shown in Fig. 7(a).

Fig. 8 shows the normalized mode III SIF, $K_{III}^{\infty}(\phi)/K_{III}^{0}(\phi = \pi/2)$, in the form of contour lines for the square (a) and the hexagonal (b) configurations as a function of angle around the crack edge, ϕ, and crack density parameter a/b for the case of $\nu = 0.3$. For the square configuration (see Fig. 1(b)), crack #3 located at distance $2b$ significantly contributes to the mode III SIF at $\phi = 90^{\circ}$ of crack #1. Correspondingly, for the hexagonal configuration (see Fig. 1(c)), crack #3 located at distance $2b$ plays a significant role in the mode III SIF at $\phi = 60^{\circ}$ (the closest point to crack #3) for high crack densities. Therefore, the maxima for the square and hexagonal configurations, respectively, occur at $\phi = 90^{\circ}$ ($\sim$2.373 at $a/b = 0.99$ in Fig. 8(a)) and $\phi = 60^{\circ}$ ($\sim$2.622 at $a/b = 0.99$ in Fig. 8(b)). For all values of a/b, the normalized mode III SIFs diminishes as ϕ approaches 0° due to the symmetry of the crack configurations with respect to the x axis. As a/b approaches zero, the normalized mode III SIF behaves as that of an isolated crack (see Eq. (27)$_2$).

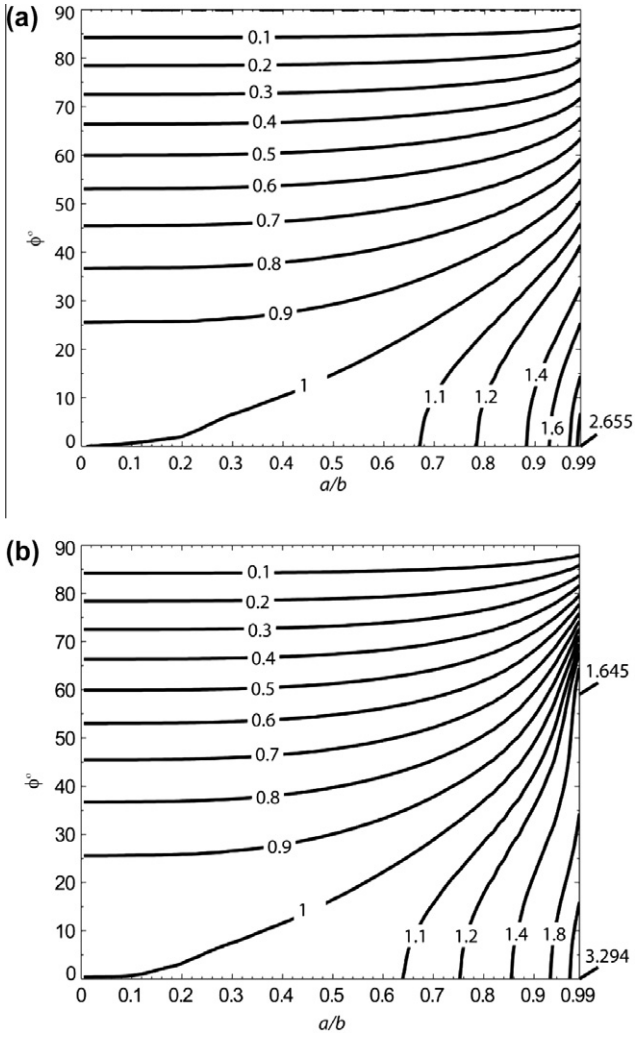

Fig. 7. Contour plot of the normalized mode II SIF, $K_{II}^{\infty}(\phi)/K_{II}^{0}(0)$, for a periodic array of coplanar penny-shaped cracks as a function of angle around the circumference, ϕ and crack density parameter a/b ($\nu = 0.3$): (a) the square (b) the hexagonal configurations. The normalization factor $K_{II}^{0}(0)$ is the SIF for an isolated crack at $\phi = 0$.

4. Discussion of the method approximations, comparison with available exact solutions

As summarized in Section 2, Kachanov's method (1994) is based on the approximation that the crack interactions are obtained from the stress distribution given by Eq. (1) for the uniformly loaded crack. In order to estimate the errors for crack interactions in a periodic array of infinite coplanar penny-shaped cracks, we select some crack interaction problems with known exact solutions and compare them against those based on Kachanov's method.

4.1. Two collinear strip cracks

Kachanov (1985) applied his approximate method to two equal collinear strip cracks in an infinite body subjected to uniform remote tension and compared the results obtained against the exact solution (Tada et al., 2000) for selected crack-to-crack distances. In order to further elucidate the nature of the approximation Fig. 9(a) shows the normalized mode I SIF at the inner and outer crack tips versus a/b in the range of $[0,0.995]$ (a is a half crack length and $2b$ is center to center distance). Dashed lines are Kachanov's approximate method and solid lines are the exact solution (Tada et al.,

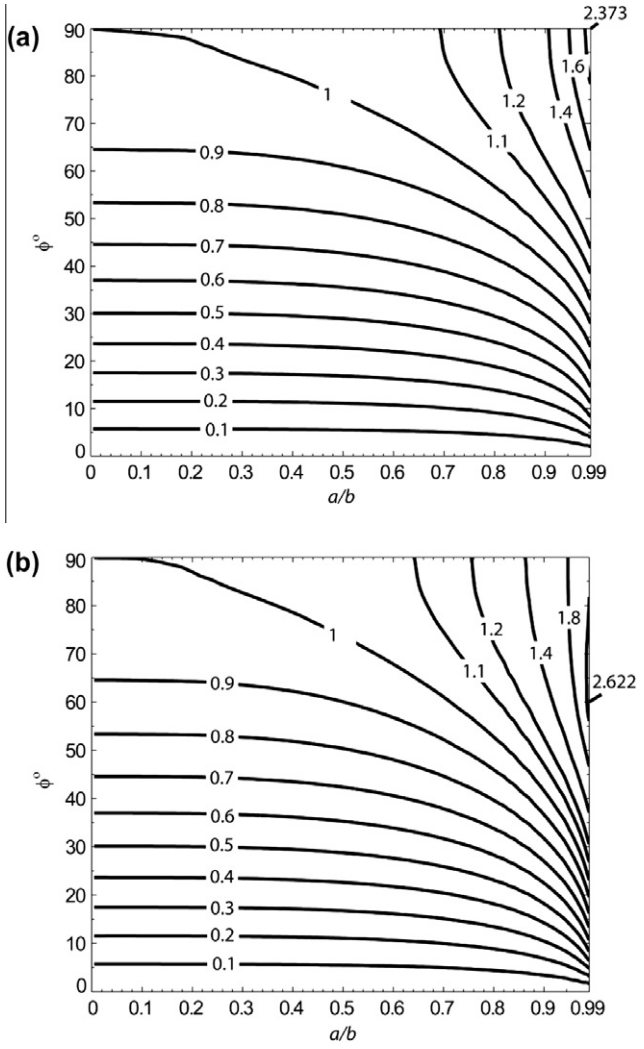

Fig. 8. Contour plot of the normalized mode III SIF, $K^{\infty}_{III}(\phi)/K^{0}_{III}(\phi=\pi/2)$,for a periodic array of coplanar penny-shaped cracks as a function of angle around the circumference, ϕ, and crack density parameter a/b ($\nu = 0.3$): (a) the square configuration (b) the hexagonal configuration. The normalization factor $K^{0}_{III}(\phi=\pi/2)$ is the SIF for an isolated crack at $\phi = \pi/2$.

2000). Note that the approximate and exact solutions for the outer crack tip are indistinguishable. The relative error in percent is shown in Fig. 9(b). As a/b increases, the relative error sharply increases and reaches the maximum value of 16.5% when a/b is 0.995 (shown as the vertical dashed line in Fig. 9(b)). The error has a negative value for both inner and outer tips indicating that the approximate method underestimates the value of mode I SIF.

4.2. Periodic array of collinear strip cracks

Kachanov (1985) also used the problem of a row of collinear strip cracks in an infinite body subjected to remote tension to verify his approximate results against the exact solution by Tada et al. (2000) for selected values of a/b. We have recomputed the results shown in Fig. 10(a) where the mode I SIF at the crack tip is shown as a function of a/b for the approximate and exact solutions. The relative error in percent is plotted in Fig. 10(b).

The percent error sharply increases as a/b approaches one and reaches the maximum error 23% when a/b is 0.995. This is larger than that for the case of two collinear cracks (16.5% when a/b is 0.995) since the crack interaction increases with the number of cracks. The sign of the error, however, is positive in an array of collinear cracks and overestimates the value of SIF as opposed to the case with two collinear cracks.

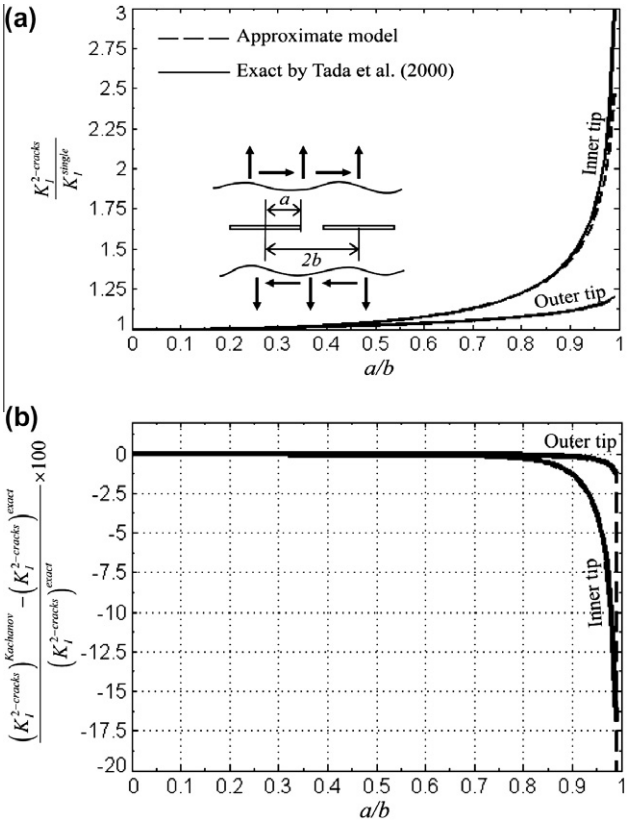

Fig. 9. (a) Comparison of the normalized mode I SIF (identical to mode II SIF) for two cracks in a homogenous medium between the approximate model (Kachanov, 1985) and the exact results by Tada et al. (2000), The normalization factor K_I^{single} is the SIF for an isolated crack. (b) Relative error (in percent) of the approximate method.

4.3. Two coplanar penny-shaped cracks

Kachanov and Laures (1989) have investigated interactions of two coplanar penny shaped cracks loaded by normal and shear stresses at infinity and compared their approximate results against the numerically evaluated exact solution of Fabrikant (1987, 1989). We have reproduced the error estimation results and have presented them in Fig. 11. The relative error for the mode I SIF increases with a/b; it remains smaller than 3.6% up to $a/b = 0.999$.

4.4. The error estimation for an array of penny-shaped cracks

Based on the error estimation discussed in Sections 4.1–4.3, errors due to Kachanov's approximate method for the case of a periodic array of penny shaped cracks outlined in Sections 2 and 3 can be approximately estimated.

As discussed by Kachanov and Laures (1989) and Kachanov (2003) crack interaction in 2 D problems is stronger than in equivalent 3D problems. In this work, the maximum values of the normalized SIFs for an array of penny-shaped cracks are shown to be approximately 3 (3.14 for the mode I SIF in Fig. 5(b) and 3.294 for the mode II SIF in Fig. 7(b)) while the corresponding quantity for an array of strip cracks is 8 (Fig. 10(a)). This, therefore, indicates that crack interactions among an array of penny-shaped cracks are likely to be much less than those among array of strip cracks.

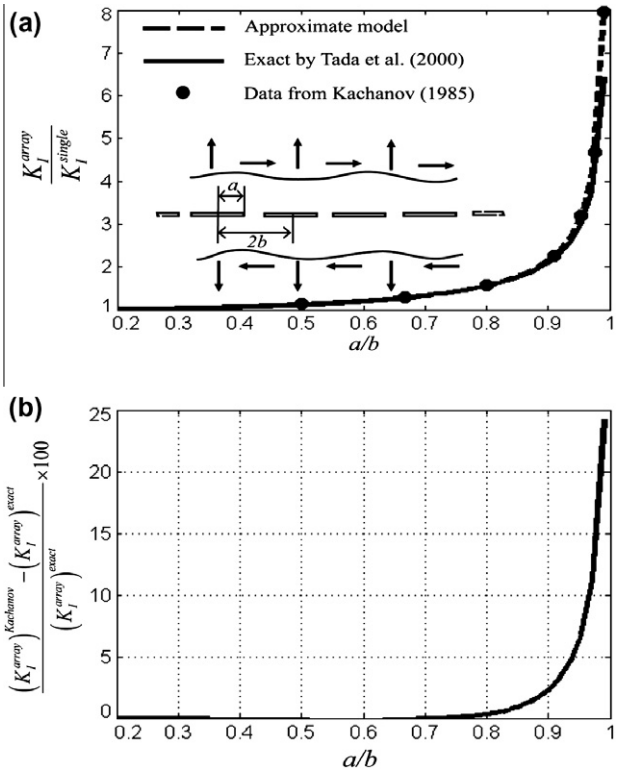

Fig. 10. (a) Comparison of the normalized mode I SIF (identical to mode II SIF) for an infinite array of cracks in a homogenous medium between the approximate model (Kachanov, 1985) and the exact results by Tada et al. (2000) The normalization factor K_I^{single} is the SIF for an isolated crack. (b) Relative error (in percent) of the approximate method.

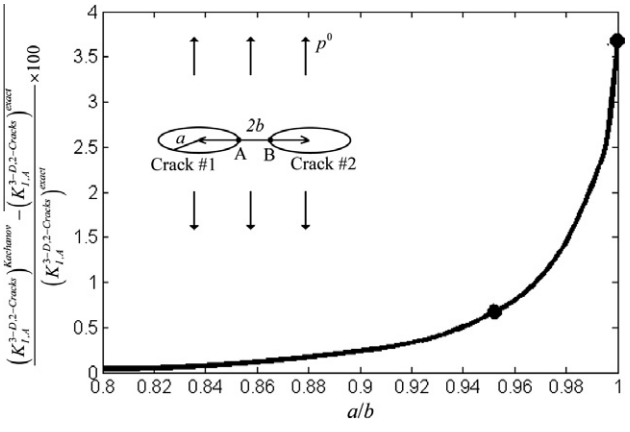

Fig. 11. The relative error in the mode I SIF of the approximate method (Kachanov and Laures, 1989) compared to the exact solution (Fabrikant, 1987, 1989) for two coplanar penny-shaped cracks as a function of a/b. The maximum error in the mode I SIF at $\phi = 0$ (circular points represent values reported on page 295 in Kachanov and Laures (1989)).

For the problem of two cracks, discussed above, the error of the approximate method for 2D cracks is 16.5% when a/b is 0.995 (Section 4.1) which is much larger than for 3D cracks that is about 2.5% up to $a/b = 0.995$, (Section 4.3). The extrapolated ratio of the errors for these two types of cracks is under 6.6. Thus it is reasonable to conjecture that the maximum error for the case of an array of coplanar penny-shaped cracks is smaller than for an array of collinear slit cracks, which is 23% when a/b is 0.995 (Section 4.2), by about the same ratio 6.6; i.e. the error is below 3.5%.

5. Approximation for widely spaced cracks

As discussed in Section 2.2, when cracks are far apart, the stress distribution induced on crack #1 by crack #j can be approximately replaced by uniform stress value at the crack #1 center. Based on this asymptotic far-field stress assumption, Kachanov derived the approximate form of the mode I SIF (Eq. (9) in Kachanov (1985)) for two coplanar cracks located away from each other. Below this approach is applied to an array of penny shaped cracks. By using the asymptotic stress, $\overline{\sigma_j}\left(\overline{\rho_j} = \frac{l_{1,j}}{a}\right) = \frac{2}{3\pi}\left(\frac{a}{l_{1,j}}\right)^3$, based on the Taylor expansion of Eq. (1) for large ρ_j and using $l_{1,j} = 2b\sqrt{p^2 + r^2}$ with $p,r = [\ldots,-2,-1,0,1,2,\ldots]$, an approximate form of the mode I SIF for the square configuration is obtained as

$$\frac{K_I^{\infty}}{K_I^0} \approx 1 + \frac{1}{12\pi}\left(\frac{a}{b}\right)^3 \left(\sum_{p=-\infty}^{\infty}\sum_{r=\infty}^{\infty}{}'(p^2+r^2)^{-3/2}\right) \approx 1 + \frac{1}{12\pi}\left(\frac{a}{b}\right)^3 (9.033). \tag{28}$$

Similarly, for the hexagonal configuration we have

$$\frac{K_I^{\infty}}{K_I^0} \approx 1 + \frac{1}{12\pi}\left(\frac{a}{b}\right)^3 \left(\sum_{p=-\infty}^{\infty}\left\{\sum_{\substack{r=-\infty \\ p:odd}}^{\infty}\left[\left(\frac{2r+1}{2}\right)^2 + \left(\frac{\sqrt{3}p}{2}\right)^2\right]^{-3/2} + \sum_{\substack{r=-\infty \\ p:even}}^{\infty}{}'\left[r^2 + \left(\frac{\sqrt{3}p}{2}\right)^2\right]^{-3/2}\right\}\right) \approx 1 + \frac{1}{12\pi}\left(\frac{a}{b}\right)^3 (11.03). \tag{29}$$

In Eqs. (28) and (29), the prime sign, $'$, indicates that the term, $p = r = 0$ is excluded in the summation. The infinite series in Eqs. (28) and (29) converges within four significant digits to 9.033 and 11.03 for the square and hexagonal configurations respectively. The second terms on the right hand side of Eqs. $(28)_2$ and $(29)_2$ show the degree of stress amplification in terms of the SIF. The converged magnification number 11.03 for the hexagonal configuration is larger than 9.033 for the square configuration, indicating the large crack interactions for the hexagonal configuration. The corresponding magnification number for two co-planar cracks is shown to be one in Eq. (9) in Kachanov (1985). It is also important to note that the SIF is constant along the crack edge. In fact, Fig. 5(a) and (b) clearly show that the normalized SIF is close to one and independent of ϕ for smaller crack density a/b.

Comparison of the approximate results based on Eqs. (28) and (29) with the results based on Eqs. (7), (9), and (10) provide the range of crack densities a/b for which Eqs. (28) and (29) may be used. The maximum error, which occurs at $\phi = 0$, remains smaller than 5% for both square and hexagonal configurations if $a/b < 0.75$.

Similarly, based on the Taylor expansion of Eq. (13) for large ρ_j, the normalized asymptotic shear stress components are given by

$$\overline{\tau_j^x}\left(\frac{l_{1,j}}{a}, \phi_j\right) \approx \frac{2}{3\pi}\left(1 + 3\frac{\nu}{2-\nu}\cos 2\phi_j\right)\left(\frac{a}{l_{1,j}}\right)^3, \tag{30}$$

$$\overline{\tau_j^y}\left(\frac{l_{1,j}}{a}, \phi_j\right) \approx \frac{2}{\pi}\left(\frac{\nu}{2-\nu}\sin 2\phi_j\right)\left(\frac{a}{l_{1,j}}\right)^3. \tag{31}$$

After summation of the contribution from all cracks, the terms with the Poisson ratio ν vanish; this is due to the periodicity of crack configurations as described in the Appendix B and an assumption of the uniform stress distribution (the stress is replaced by that at crack #1 center). This leads to a significant simplification where the approximate normalized mode II and III SIFs are shown to be identical to those for the mode I SIFs as follows.

$$\frac{K_{II}^{\infty}(\phi)}{K_{II}^{0}(\phi)} = \frac{K_{III}^{\infty}(\phi)}{K_{III}^{0}(\phi)} \approx 1 + \frac{1}{12\pi}\left(\frac{a}{b}\right)^3 (9.033) \tag{32}$$

for the square configuration and

$$\frac{K_{II}^{\infty}(\phi)}{K_{II}^{0}(\phi)} = \frac{K_{III}^{\infty}(\phi)}{K_{III}^{0}(\phi)} \approx 1 + \frac{1}{12\pi}\left(\frac{a}{b}\right)^3 (11.03) \tag{33}$$

for the hexagonal configuration.

It is important to note that while Eqs. (32) and (33) are independent of ϕ, the dependence of K_{II}^{∞} and K_{III}^{∞} on ϕ comes in through cos (ϕ) and sin (ϕ), respectively, as in the single crack case (see Eq. (27)).

Errors due to the widely-spaced-cracks approximation (Eqs. (32) and (33)) are evaluated by comparing them with Eq. (24) and it is shown that the maximum percent error remains smaller than 6% for all Poisson's ratio values when $a/b < 0.75$.

6. Comparison with prior work

In this section, we compare some of our obtained results with the existing work available in the literature. Sekine and Mura (1979) investigated the three-dimensional stress field for a periodic array of penny-shaped cracks in an infinite isotropic elastic solid under arbitrary uniform loadings based on the Somigliana dislocation method. The displacement discontinuity of the Somigliana dislocations is assumed to be in the form $p(x_1', x_2')[1-(x_1')^2-(x_2')^2]^{1/2}$. The coefficients of the polynomial $p(x_1', x_2')$ are determined using the boundary conditions on the surfaces of the penny-shaped cracks where the stresses on the crack surfaces are zero. Numerical results for the stress intensity factors are obtained for the square configuration shown in Fig. 1(b). They obtained the maximum values of the normalized mode I SIF as a function of crack density a/b ranging from 0.4 to 0.92 (Fig. 5 in Sekine and Mura (1979)). In Fig. 12, the corresponding results of this work (solid line) are compared with their results (dashed line). As shown in the figure, the relative percent difference between the two methods remains less than 2.8%.

They also obtained the normalized mode II and mode III SIFs as a function of angle ϕ for two different values of a/b (0.8333, 0.6667) with $\nu = 0.3$ (Fig. 3 in Sekine and Mura (1979)). In Fig. 13, the corresponding results in this work are compared with their results, and it is found that the relative percent difference between the two methods is less than 1%.

The numerical results by Sekine and Mura (1979) are approximate in the sense that they are obtained by truncating the series for the displacement gradients; they did not investigate the effect of this truncation. The results obtained in this work also involve approximations as outlined in Sections 2 and 3. The minor discrepancy between two methods may be attributed to the different nature of the approximations and numerical errors.

By modeling discontinuous macro-flaws by a periodic array of coplanar periodic shaped cracks, Huang and Karihaloo (1992) investigated the so-called tension softening regime of quasi-brittle materials which exhibits moderate strain hardening behavior before ultimate failure. By assuming cracks grow in a self-similar manner, they examined the reduction in the stress transfer capacity with increasing deformation. Their analysis is based on a Fredholm integral equation of the second kind and formulation through displacement averages instead of traction averages (Kachanov, 1985). The average mode I stress intensity factor defined by

$$\langle K_I(\phi)\rangle = \frac{1}{2\pi}\int_0^{2\pi} K_I(\phi)\,d\phi, \tag{34}$$

was numerically obtained as a function of crack density, a/b, in Table 6 in Huang and Karihaloo (1992).

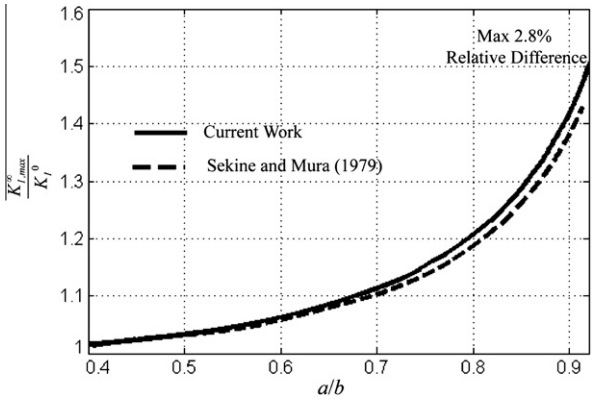

Fig. 12. Comparison of the maximum values of normalized mode I SIF calculated in current work and those produced by Sekine and Mura (1979) for periodic (square) array of coplanar penny-shaped cracks.

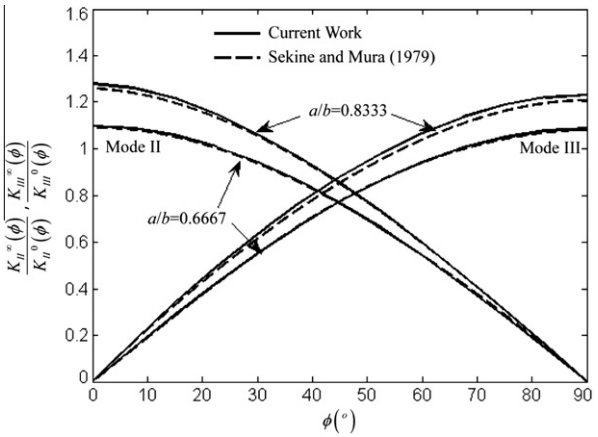

Fig. 13. Comparison of the normalized mode II and mode III SIF around the crack edge based on two methods for two different a/b ratio, 0.6667 and 0.8333 ($\nu = 0.3$).

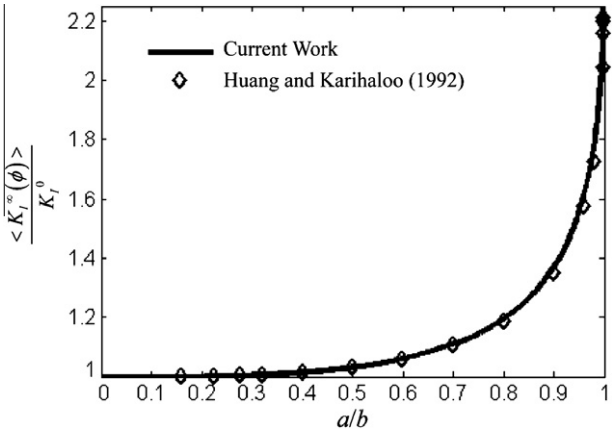

Fig. 14. Comparison of the averaged value of normalized mode I SIF as a function of a/b calculated in current work and calculated values based on Huang and Karihaloo (1992) for square configuration of a periodic array of coplanar penny-shaped cracks.

In Fig. 14, their results (diamond-shaped points) are compared against those obtained in this work (solid line). As can be seen from the figure, the two solutions are indistinguishable for even very high crack densities. While comparison with prior work is limited to the special cases, good agreement with the existing results as demonstrated in Figs. 12–14 provides support for the accuracy of the results presented.

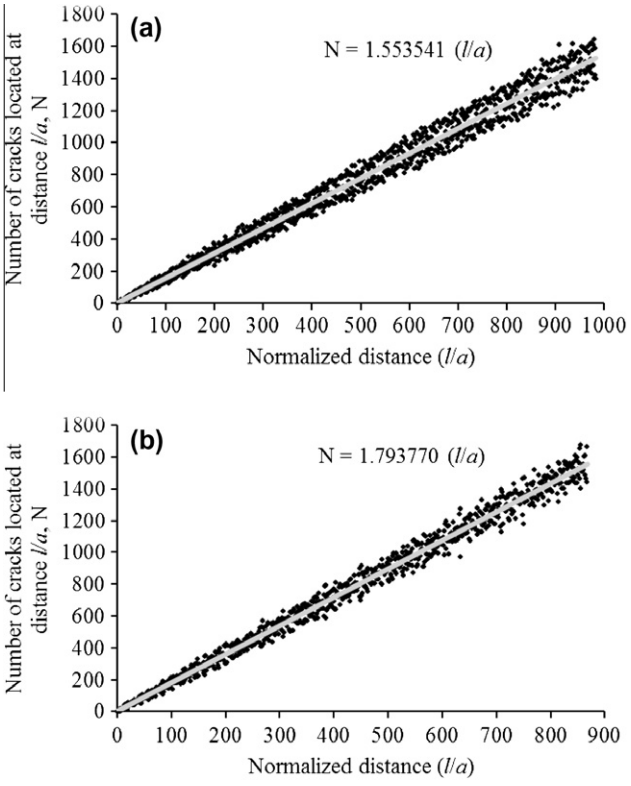

Fig. 15. Number of cracks located at distance l/*a*, *N*, versus the normalized distance l/*a* for a/b = 0.99 (a) for the square crack configuration (b) for the hexagonal crack configuration.

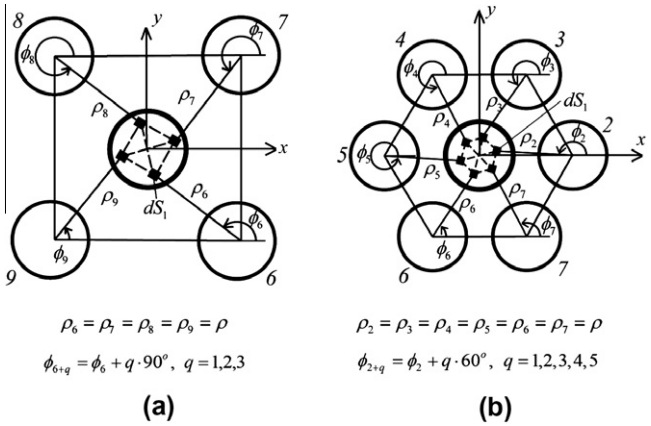

Fig. 16. (a) Four infinitesimal areal elements (black squares) squarely located within crack #1 region corresponding to crack #6, 7, 8, 9; (b) Six infinitesimal areal elements hexagonally located within crack #1 region corresponding to crack #2, 3, 4, 5, 6, 7.

7. Summary and conclusions

In this work, stress intensity factors (SIFs) for a doubly periodic array of coplanar penny-shaped cracks are examined for square and hexagonal crack configurations based on Kachanov's approximate method for crack interactions (1994). Due to the periodicity of the crack array, the unknown average traction is the same for all cracks; that allows us to obtain the normalized averaged crack traction factored by the term $1/(1-\sum_{j=2}^{\infty} A_{j1}^{zz})$, which may be interpreted as an amplification factor due to crack interactions.

The periodicity and symmetry of crack array patterns is shown to play an important role in significantly simplifying the formulation for transverse load. In particular, the summation of transmission factors for the shear mode is shown to be independent of Poisson's ratio for square and hexagonal crack configurations even though the crack-generated stress field depends on it. This is because for an arbitrary chosen crack in the infinite arrays of square and hexagonal crack configurations, there exist multiple rows of four (for the square configuration) or six (for the hexagonal configuration) cracks located at the same distance from the chosen crack, thus forming squares or hexagons. This allows us to demonstrate that the average traction amplification factor for the transverse traction is identical to that for the normal traction.

Convergence of solutions is investigated in terms of the truncation number *m* of the total number of cracks and is found to be very slow; for this reason in computations the non-homogeneous stress distribution over crack #1 due to the action of a remote crack *j* is replaced by a constant (this is determined by a transition number *n*). The detailed numerical analysis results in selecting the truncation number $m = 10^9$ and the transition numbers $n = 25$ and 31 for the square and hexagonal configurations respectively. The convergence error for SIFs at $a/b = 0.99$ (the highest crack density considered) and $\nu = .5$ (the highest error) is found to be less than 0.09%.

At first sight the slow convergence with *m* may be surprising since the stress generated by a single crack decays asymptotically as the inverse of distance cubed. However, since the number of cracks increases linearly with distance from the central crack, the total stress created by all the cracks decays as the inverse of distance squared. It is shown that after integrating over the annular area bounded by two distinct radii, the summation of stress created by all the cracks located within this annular area decay as the inverse of the distance.

By surface fitting the numerical results, empirical normalized mode I SIF equations are obtained as functions of crack density ($0 < a/b < 0.99$) and angle around the crack edge. For the normalized mode II and III SIFs, numerical results for $\nu = 0.3$ are presented in the form of contour lines as a function of crack density and angle around the crack edge. These empirical equations and contour plot data can be used to estimate the SIFs for both square and hexagonal crack configurations for most materials.

Possible errors due to Kachanov's approximation method with regards to the obtained SIF data are roughly estimated to be less than 3.5% based on the known errors for the cases of two 2D cracks, a periodic array of 2D cracks, and two 3D (penny-shaped) cracks.

For $a/b < 0.7$, the widely-spaced-crack approximation based on the asymptotic far-field stress approximation is employed with less than 6% error for all Poisson's ratio values. The appropriately normalized mode I, II and III SIFs are shown to be identical and

Table 1
The increase in the normalized crack-generated stresses due to the increase in the total crack number from 10^9 to 10^{10}: comparison of the asymptotic (Eq. A3) and computed $\sum_{j=10^9}^{10^{10}} \bar{\sigma}_j(0,0)$ with exact terms.

	Square crack configuration	Hexagonal crack configuration
η	1.553541	1.793770
Asymptotic $\frac{2\eta}{3\pi}\left(\frac{a}{l}(at\ m = 10^9) - \frac{a}{l}(at\ m = 10^{10})\right)$	6.25 (10^{-6})	7.76 (10^{-6})
$\sum_{j=10^9}^{10^{10}} \bar{\sigma}_j(0,0)$	6.20 (10^{-6})	7.70 (10^{-6})

dependent on crack density only. The crack edge angle dependence of mode II and III SIFs comes from the normalization factor by the SIF of a single crack. The degree of SIF amplification for the hexagonal configuration is found to be higher than that for the square configuration, indicating stronger crack interactions.

Some of our results are compared with the limited existing work done by other methods found in the literature, and good agreement with the existing results is obtained, demonstrating the accuracy of our obtained results.

Acknowledgements

The authors acknowledge partial support of this research by NIHDCR C R21 DEO14719-0 Grant; SIR also acknowledges partial support by NASA NNX08BA37A Grant.

Appendix A. Analysis of convergence of crack-generated stresses due to truncation of total crack number *m*

This appendix explores the reason why a large number of cracks is required for the convergence of crack-generated stresses by considering the total number of cracks located within the circular region. Recall Eq. (1),

$$\overline{\sigma_j}(\overline{\rho_j}) = \frac{2}{\pi}\left[\frac{1}{\sqrt{\overline{\rho_j}^2-1}} - \sin^{-1}\left(\frac{1}{\overline{\rho_j}}\right)\right],$$

where $\overline{\rho_j} = \rho_j/a$ and ρ_j is the radial distance measured from the center of crack #*j*.

Based on the Taylor expansion of Eq. (1) for large ρ_j, the asymptotic stress field decays as the distance cubed as follows.

$$\overline{\sigma_j}\left(\overline{\rho_j} = \frac{l_{1,j}}{a}\right) = \frac{2}{3\pi}\left(\frac{l_{1,j}}{a}\right)^{-3}. \tag{A1}$$

For a periodic array of coplanar cracks, the number of cracks located at the distance ℓ from crack #1 center is approximately proportional to distance ℓ; we normalize the distance by crack radius *a*. Since the convergence of the normalized stress is slowest when the crack density is highest, we consider the case $a/b = 0.99$. The number of cracks located at the normalized distance ℓ/a is shown by discrete points in Fig. 15(a) and (b) for the square and hexagonal configurations correspondingly. The linear proportionality constant denoted by η is determined by curve fitting; $\eta = 1.553541$ for the square and $\eta = 1.793770$ for the hexagonal configurations.

The summation of the normalized asymptotic stress $\bar{\sigma}$ for number of cracks $\eta(\ell/a)$ at the normalized distance ℓ/a can be expressed as

$$\sum_{j=1}^{\eta\left(\frac{l}{a}\right)} \bar{\sigma}_j = \frac{2}{3\pi}\left(\frac{l}{a}\right)^{-3} \times \eta\left(\frac{l}{a}\right) = \frac{2\eta}{3\pi}\left(\frac{l}{a}\right)^{-2}. \tag{A2}$$

When the normalized distance ℓ/a is increased from ℓ_1/a to ℓ_2/a ($\ell_2 > \ell_1$), the increase in the normalized asymptotic stress is obtained approximately by integrating Eq. (A2)

$$\int_{\frac{l_1}{a}}^{\frac{l_2}{a}} \frac{2\eta}{3\pi}\left(\frac{l}{a}\right)^{-2} d\left(\frac{l}{a}\right) = \frac{2\eta}{3\pi}\left(\frac{a}{l_1} - \frac{a}{l_2}\right). \tag{A3}$$

Based on the asymptotic stress field it follows from Eq. (A3) that crack-generated stresses in the array decay as the inverse of the distance.

Indeed comparison of Eq. (A3) with the numeric calculations shows that it provides good estimates of stress decay for both crack configurations: as an example Table 1 lists the exact increase of crack-generated stresses for crack number increase from 10^9 to $10^{10}\sum_{j=10^9}^{10^{10}} \bar{\sigma}_j(0,0)$ (without the asymptotic stress field assumption) and that obtained by asymptotic Eq. (A3) for the normalized distances ℓ_1/a and ℓ_2/a corresponding to total crack number $m = 10^9$ and 10^{10}.

In summary, while crack #*j* generated normalized stress asymptotically decays as the inverse of distance cubed as in Eq. (A1), the number of cracks located at the distance ℓ/a increases linearly with distance (see Fig. 15(a) and (b)). Therefore, the crack-generated stresses at distance ℓ/a decay as the inverse of distance squared as in Eq. (A2). After summing the stresses generated by cracks located within the annular region bounded by distance ℓ_1/a and ℓ_2/a ($\ell_2 > \ell_1$), we obtain Eq. (A3), indicating that the crack-generated stresses decays as the inverse of the distance. Therefore the convergence is very slow.

Appendix B. Independence of summation of transmission factors on Poisson's ratio for mode II and III SIFs due to periodicity of crack configurations

B.1. Square configuration

The distance between crack #1 with the center located at $C_1(0,0)$ and crack #*j* with the center located at $C_j(2br,2bp)(p,r = [\ldots,-2,-1,0,1,2,\ldots])$ is given by

$$l_{1,j} = 2b\sqrt{r^2+p^2} \tag{B1}$$

and the angle between the *x* axis and the line connecting points $C_1(0,0)$, $C_j(2br,2bp)$ (see Fig. 2) can be written as

$$\psi_{1j} = \tan^{-1}\left(\frac{p}{r}\right). \tag{B2}$$

In the square configuration, there is a multiple of four cracks located at the same distance $l_{1,j}$. For example, if we choose crack #6 corresponding to the pair $r = 1$ and $p = -1$, the crack distance is $l_{1,6} = 2\sqrt{2}b$ and the three other cracks (crack #7, 8, 9 corresponding to $(r,p) = (1,1)$, $(-1,1)$ and $(-1,-1)$, respectively) also have $l_{1,j} = 2\sqrt{2}b$ ($j = 7,8,9$). As can be calculated from Eq. (B2), the difference of the angle ψ_{1j} between two adjacent cracks among these four cracks is 90°. From Eq. (16), the summation of A_{j1}^{xy} or A_{j1}^{yx} for these four cracks can be expressed as follows:

$$\sum_{j=6,7,8,9} A_{j1}^{xy} = \sum_{j=6,7,8,9} A_{j1}^{yx} = \frac{2}{\pi^2 a^2}\left(\frac{v}{2-v}\right)\int\int_{S_1}\sum_{j=6,7,8,9}\frac{\sin 2\phi_j}{\bar{\rho}_j^2\sqrt{\bar{\rho}_j^2-1}}dS_1. \tag{B3}$$

Similarly, from Eqs. (1) and (2), the first terms on the right hand side of Eq. (17)$_{1,2}$ for A_{j1}^{xx} and A_{j1}^{yy} are equal to A_{j1}^{zz}. Utilizing this equality in the summation of these terms for the four cracks, we have

$$\sum_{j=6,7,8,9} A_{j1}^{xx} = \sum_{j=6,7,8,9} A_{j1}^{zz} + \frac{2}{\pi^2 a^2}\left(\frac{v}{2-v}\right)\int\int_{S_1}\sum_{j=6,7,8,9}\frac{\cos 2\phi_j}{\bar{\rho}_j^2\sqrt{\bar{\rho}_j^2-1}}dS_1,$$

$$\sum_{j=6,7,8,9} A_{j1}^{yy} = \sum_{j=6,7,8,9} A_{j1}^{zz} - \frac{2}{\pi^2 a^2}\left(\frac{v}{2-v}\right)\int\int_{S_1}\sum_{j=6,7,8,9}\frac{\cos 2\phi_j}{\bar{\rho}_j^2\sqrt{\bar{\rho}_j^2-1}}dS_1. \tag{B4}$$

Fig. 16(a), shows an arbitrary infinitesimal areal element dS_1, located on a surface of crack #1 at radius ρ_6 nd angle ϕ_6 measured from crack #6 together with three other infinitesimal elements, dS_1, located at (ρ_7,ϕ_7), (ρ_8,ϕ_8), and (ρ_9,ϕ_9) and measured from crack #7, 8 and 9 respectively. Those elements can be chosen so

that the distances ρ_6, ρ_7, ρ_8, and ρ_9, are the same and the corresponding angles ϕ_6, ϕ_7, ϕ_8 and ϕ_9 are related by multiples of 90° as follows.

$$\rho_6 = \rho_7 = \rho_8 = \rho_9 = \rho, \tag{B5}$$
$$\phi_{6+q} = \phi_6 + q \cdot 90^\circ, \quad q = 1,2,3. \tag{B6}$$

The special relation among angles as shown in Eq. (B6) leads to

$$\sum_{j=6,7,8,9} \cos 2\phi_j = \sum_{q=0}^{3} \cos(2(\phi_6 + q \cdot 90^\circ))$$
$$= \cos(2\phi_6) \sum_{q=0}^{3} \cos(2 \cdot q \cdot 90^\circ) = 0,$$
$$\sum_{j=6,7,8,9} \sin 2\phi_j = \sum_{q=0}^{3} \sin(2(\phi_6 + q \cdot 90^\circ))$$
$$= \sin(2\phi_6) \sum_{q=0}^{3} \cos(2 \cdot q \cdot 90^\circ) = 0. \tag{B7}$$

Recalling the normalized radius $\bar{\rho}_j = \frac{\rho_j}{a}$, the summation terms, $\sum_{j=6,7,8,9} \frac{\cos 2\phi_j}{\bar{\rho}_j^2 \sqrt{\bar{\rho}_j^2 - 1}} dS_1$ and $\sum_{j=6,7,8,9} \frac{\sin 2\phi_j}{\bar{\rho}_j^2 \sqrt{\bar{\rho}_j^2 - 1}} dS_1$, for the four squarely located infinitesimal areal elements then vanish due to Eqs. (B5) and (B7). Integration of these summation terms over the entire crack #1 region, which appears on the right hand side of Eq. (B3) and in the second terms of the right hand side of Eq. (B4), therefore, also vanish, and Eqs. (B3) and (B4) are now simplified as follows:

$$\sum_{j=6,7,8,9} \Lambda_{j1}^{xy} = \sum_{j=6,7,8,9} \Lambda_{j1}^{yx} = 0, \quad \sum_{j=6,7,8,9} \Lambda_{j1}^{xx} = \sum_{j=6,7,8,9} \Lambda_{j1}^{yy} = \sum_{j=6,7,8,9} \Lambda_{j1}^{zz}, \tag{B8}$$

where the summation of transmission factors in the shear mode for crack #6,7,8, and 9 becomes independent of Poisson's ratio. By applying this procedure to multiple rows of four cracks squarely located at the same distance, Eq. (B8) can be extended to the case for an infinite number of cracks for the square crack configuration, and we obtain Eq. (21).

In summary, for the square crack configuration there are multiple rows of squarely located four cracks at the same distance from crack #1. As shown in Fig. 16(a), one can select squarely located four infinitesimal areal elements within the crack #1 region, related to the surrounding squarely located four cracks (crack #6, 7, 8 and 9), such that they satisfy the special conditions of having identical radial distances and angles related by a multiple of 90° as in Eqs. (B5) and (B6). These special conditions lead to Poisson's ratio effect cancelation in the summation of transmission factors for the shear mode loading. Therefore, the periodicity of the square crack configuration plays a key role in obtaining Eq. (21).

B.2. Hexagonal configuration

Similarly, we will show that the summation of transmission factors in the shear mode for the hexagonal configuration (Fig. 16(b)) also becomes independent of Poisson's ratio.

The distance between crack #1 with center located at $C_1(0,0)$ and crack #j with center located at $C_j\left(2b\frac{2r+1}{2}, 2b\frac{\sqrt{3}p}{2}\right)(p: odd)$ or $C_j\left(2br, 2b\frac{\sqrt{3}p}{2}\right)(p: even)$ [$p,r = \ldots -2,-1,0,1,2,..$, excluding $r = p = 0$] is given by

$$l_{1j} = \begin{cases} 2b\sqrt{\left(\frac{2r+1}{2}\right)^2 + \left(\frac{\sqrt{3}p}{2}\right)^2} & p: odd, \\ 2b\sqrt{r^2 + \left(\frac{\sqrt{3}p}{2}\right)^2} & p: even \end{cases} \tag{B9}$$

and the angle between the line connecting $C_1(0,0)$, $C_j\left(2b\frac{2r+1}{2}, 2b\frac{\sqrt{3}p}{2}\right)(p: odd)$ or $C_j\left(2br, 2b\frac{\sqrt{3}p}{2}\right)(p: even)$ and the x axis can be written as

$$\psi_{1j} = \begin{cases} \tan^{-1}\left(\frac{\sqrt{3}p}{2r+1}\right) & p: odd, \\ \tan^{-1}\left(\frac{\sqrt{3}p}{2r}\right) & p: even. \end{cases} \tag{B10}$$

In the hexagonal configuration, there is a multiple of six cracks located at the same distance l_{1j}. For example, if we choose crack #2 corresponding to the pair at $r = 1$ and $p = 0$, the crack distance is $l_{1,2} = 2b$ and the five others, cracks #3,4,5,6,7, corresponding to $(r,p) = (0,1),(-1,1),(-1,0),(-1,-1)$ and $(1,-1)$, respectively, also have $l_{1j} = 2b$. As can be calculated from Eq. (B10), the angle between these consecutive points is 60°.

As in the example of square crack configuration, one selects on the crack #1 surface an arbitrary (Fig. 16(b)) infinitesimal areal element dS_1, defined in the coordinate system ρ_2, ϕ_2 entered at crack #2, together with five other infinitesimal elements, dS_1, located at coordinates (ρ_3,ϕ_3), (ρ_4,ϕ_4), (ρ_5,ϕ_5), (ρ_6,ϕ_6) and (ρ_7,ϕ_7) measured from crack # 3, 4, 5, 6, and 7 respectively. Due to the hexagonal formation of cracks, the distances ρ_i are identical and the angles are related with multiples of 60°:

$$\rho_2 = \rho_3 = \rho_4 = \rho_5 = \rho_6 = \rho_7 = \rho, \tag{B11}$$
$$\phi_{2+q} = \phi_2 + q \cdot 60^\circ, \quad q = 1,2,3,4,5. \tag{B12}$$

Eq. (B12) leads to:

$$\sum_{j=2,3,4,5,6,7} \cos 2\phi_j = \sum_{q=0}^{5} \cos(2(\phi_2 + q \cdot 60^\circ)) = 0,$$
$$\sum_{j=2,3,4,5,6,7} \sin 2\phi_j = \sum_{q=0}^{5} \sin(2(\phi_2 + q \cdot 60^\circ)) = 0. \tag{B13}$$

As in Eqs.(B8) for the square configuration, Eqs. (B11) and (B13) again lead to equalities

$$\sum_{j=2,3,4,5,6,7} \Lambda_{j1}^{xy} = \sum_{j=2,3,4,5,6,7} \Lambda_{j1}^{yx} = 0, \quad \sum_{j=2,3,4,5,6,7} \Lambda_{j1}^{xx} = \sum_{j=2,3,4,5,6,7} \Lambda_{j1}^{yy} = \sum_{j=2,3,4,5,6,7} \Lambda_{j1}^{zz} \tag{B14}$$

and as a result the summation of transmission factors in the shear mode of cracks #2, 3, 4, 5, 6, and 7 become independent of Poisson's ratio. As in the square configuration, by applying this procedure to multiple rows of six cracks hexagonally located at the same distance Eq. (B14) can be extended to the case of an infinite number of cracks and we obtain Eq. (21) for the hexagonal crack configuration.

B.3. Other polygonal crack configurations

As long as we have n cracks which are located to form an n-polygon with the central crack #1, n infinitesimal areal elements dS_1 can be assembled to form the same n-polygon within crack region #1 with properties similar to Eqs. (B5), (B6), (B11) and (B12). However, only square and hexagonal crack configurations satisfy the periodicity of crack patterns where any arbitrary crack can be chosen to be the center crack #1. This periodicity is essential in our proof of the average stress equality, Eq. (19), for an infinite number of cracks. Therefore, the independence of Poisson's ratio of the summation of transmission factors in the shear mode for an array of periodic cracks can be proven by the current method, and most likely exists, for only square and hexagonal crack configurations.

References

Fabrikant, V.I., 1987. Close interaction of coplanar circular cracks in an elastic medium. Acta Mechanica 67 (1–4), 39–59.

Fabrikant, V.I., 1989. Close interaction of coplanar circular cracks under shear loading. Computational Mechanics 4, 181–197.

Fabrikant, V.I., 1990. Complete solutions to some mixed boundary-value-problems in elasticity. Advances in Applied Mechanics 27, 153–223.

Huang, X., Karihaloo, B.L., 1992. Tension softening of quasi-brittle materials modeled by singly and doubly periodic arrays of coplanar penny-shaped cracks. Mechanics of Materials 13 (3), 257–275.

Kachanov, M., 1985. A simple technique of stress-analysis in elastic solids with many cracks. International Journal of Fracture 28 (1), R11–R19.

Kachanov, M., 1987. Elastic solids with many cracks: a simple method of analysis. International Journal of Solids and Structures 23 (1), 23–43.

Kachanov, M., 1994. Elastic solids with many cracks and related problems. Advances in Applied Mechanics 30, 259–445.

Kachanov, M., 2003. On the problems of cracks interactions and crack coalescence. International Journal of Fracture 120, 537–543.

Kachanov, M., Laures, J.P., 1989. 3-Dimensional problems of strongly interacting arbitrarily located penny-shaped cracks. International Journal of Fracture 41 (4), 289–313.

Lavrentyev, A.I., Rokhlin, S.I., 1994. Models for ultrasonic characterization of environmental degradation of interfaces in adhesive joints. Journal of Applied Physics 76 (8), 4643–4650.

Sankar, T.S., Fabrikant, V.I., 1983. Punch and crack problems in transversely isotropic bodies. International Journal of Engineering Science 21 (7), 799–811.

Sekine, H., Mura, T., 1979. Weakening of an elastic solid by a periodic array of penny-shaped cracks. International Journal of Solids and Structures 15 (6), 493–502.

Sneddon, I.N., Lowengrub, M., 1969. Crack Problems in the Classical Theory of Elascitity. Wiley, New York, NY.

Tada, H., Paris, P.C., Irwin, G.R., 2000. The Stress Analysis of Cracks Handbook. ASME Press, New York, NY.

Zhan, S.G., Wang, T.C., 2006. Interactions of penny-shaped cracks in three-dimensional solids. Acta Mechanica Sinica 22 (4), 341–353.